A&A 480, 527–536 (2008)
DOI: 10.1051/0004-6361:20078826

Astronomy & Astrophysics

Formation of suprathermal electron distributions in the quiet solar corona

C. Vocks, G. Mann, and G. Rausche

Astrophysikalisches Institut Potsdam, An der Sternwarte 16, 14482 Potsdam, Germany
e-mail: cvocks@aip.de

Received 10 October 2007 / Accepted 21 December 2007

ABSTRACT

Context. Solar wind electron velocity distribution functions (VDFs) show enhanced levels of suprathermal electrons as compared to a Maxwellian distribution. Previous studies show that the suprathermal tails of solar wind VDFs can be fitted by kappa distributions, and that a coronal origin of the suprathermal electrons is possible.
Aims. The generation of suprathermal electrons by resonant interaction with whistler waves in the corona is investigated under quiet solar conditions without any flare activity. The magnetic field geometry is that of a closed magnetic loop. The electron-whistler interaction is described within the framework of quasilinear theory, that leads to pitch-angle diffusion of the electrons in the reference frame of the waves.
Methods. A study of electron VDFs requires a kinetic description of the electrons. The model used in this paper is based on a numerical solution of the Boltzmann-Vlasov equation for the electrons, considering Coulomb collisions and wave-electron interaction. The waves are assumed to enter the simulation box with a given power-law spectrum, which evolves inside the box due to wave propagation and absorption by the electrons. Starting from a nearly Maxwellian initial electron VDF, the temporal evolution of the VDF is calculated until a final steady state has been reached.
Results. The results show that a population of suprathermal electrons develops in a closed coronal loop. The electron VDF can be approximated by a power-law in the energy range of 4–10 keV. The power-law index is in agreement with the solar wind observations. For lower energy, the electrons are thermalized in the dense model coronal loop, and the efficiency of the acceleration mechanism decreases for higher energies. The energy range of the simulation box has to be chosen sufficiently large, and the influence of the loop geometry on the results is also studied.
Conclusions. These numerical studies show that the quiet solar corona is capable of producing suprathermal electron VDFs with similar characteristics to those observed in the solar wind. This study is focused on a closed region in the solar corona, but if such an electron population is present in the corona, it should also appear in the solar wind.

Key words. acceleration of particles – plasmas – waves – methods: numerical – Sun: corona – Sun: solar wind

1. Introduction

Observations of solar wind electrons show distinct deviations from a simple Maxwellian velocity distribution function (VDF). Strong suprathermal tails are observed even under quiet solar conditions (Lin 1980). Different components can be distinguished: a thermal core, a halo distribution with electron energies of a few keV, and a more energetic superhalo (Lin 1998). The core and superhalo are isotropic, but the halo component shows a strong anisotropy with a beam or "strahl" directed away from the Sun (Pilipp et al. 1987). A description of the core and halo distributions as the sum of two Maxwellian VDFs with different temperatures seems to be straightforward. But Maksimovic et al. (1997a) have found that electron VDFs in interplanetary space can be fitted better by so-called kappa distributions. Kappa distributions are discussed as equilibrium states in nonextensive thermostatics (Leubner 2004), which justifies their use for solar wind electron VDFs.

The presence of suprathermal tails in solar wind electron VDFs raises the question of where and how these electrons are accelerated. Does it happen in the solar wind, or are the suprathermal tails already formed in the corona? Pierrard et al. (1999) have calculated the coronal electron distributions that lead to solar wind electron VDFs as observed by the WIND spacecraft at 1 AU. They found that a coronal origin of the suprathermal tails is possible.

To describe the evolution of electron VDFs, a kinetic model is needed. For the solar corona and wind, several kinetic models exist. Scudder (1992a,b) investigates the role suprathermal electrons play in the corona and finds that they can have significant impact on the thermal structure of the corona through the velocity filtration mechanism. Lie-Svendsen et al. (1997) and Lie-Svendsen & Leer (2000) developed an exospheric model to study the evolution of electron VDFs from the corona into interplanetary space. This model includes Coulomb collisions, but no mechanism to scatter or accelerate suprathermal electrons in the corona or solar wind. The model starts with a Maxwellian VDF in the corona. The solar wind solution shows a beam of electrons directed away from the Sun, but not the strong suprathermal tails as they are observed. Maksimovic et al. (1997b) use a kappa distribution for the coronal electrons in their exospheric model and yield results that are in better agreement with observed solar wind parameters. Dorelli & Scudder (2004) assess the consequences of electron kappa distributions in the corona on the heat flux. They find that heat fluxes against the local temperature gradient are possible, and discuss the implications for coronal heating models.

Vocks & Mann (2003) have developed a kinetic model for electrons in the solar corona and wind in order to investigate whether it is possible to produce suprathermal electrons in the quiet corona, starting with a nearly Maxwellian electron VDF.

The electron acceleration is based on resonant interaction between electrons and whistler waves. The whistler waves are assumed to be the high-frequency tail of a wave spectrum that is also discussed for coronal heating (e.g. Cranmer et al. 1999; Vocks & Marsch 2002). Under quiet solar conditions without major flare activity, the wave spectrum is generated in the chromospheric network (Axford et al. 1999) and propagates upwards into the corona and thus into the computational domain. The results indeed show enhanced fluxes of suprathermal electrons, and thus demonstrate that the quiet solar corona is capable of generating enhanced numbers of suprathermal electrons. But these model calculations did not investigate either whether a kappa-like electron VDF forms, or the shape of the suprathermal tails. Furthermore, the model was restricted to low electron energies of a few keV. This model is used in Vocks & Mann (2005) to study the evolution of an electron VDF in the solar wind. These calculations reproduce the observed features of solar wind VDFs, i.e. core, halo, and strahl components, but they are also limited to an electron energy of 6 keV, so superhalo energies are not covered by the model.

These kinetic model calculations show that the corona is capable of producing an enhanced number of suprathermal electrons compared to a Maxwellian VDF, even under quiet solar conditions without any flare activity. But they did not provide a quantitative analysis of the suprathermal electron population, and did not study whether its distribution forms a power law and can be fitted by a kappa distribution. Furthermore, a more comprehensive analysis of this electron acceleration mechanism requires an extension of the model to higher energies. In the solar wind, suprathermal electrons are observed up to 100 keV (Lin 1998), so this energy range should be covered.

This paper provides a more detailed analysis of the evolution of coronal electron VDFs under the influence of resonant interaction with whistler waves. The energy range is extended to more than 100 keV. The model calculations start as in the previous papers with a nearly Maxwellian VDF, i.e. a kappa distribution with $\kappa = 80$, in order to ensure that it is indeed the whistlers, and not some initial or boundary condition that leads to suprathermal tail formation. The geometry of the simulation box is a closed coronal loop, and not a coronal hole as in Vocks & Mann (2003), that is open towards interplanetary space. The closed geometry has the advantage that it enables a study focused on the physical processes in the corona, without the need to either define an upper boundary condition for the electron VDF in the corona, or extend the model into the solar wind.

2. The model

The kinetic model for electrons in the solar corona used in this paper is an extension of the model presented by Vocks & Mann (2003). These earlier model calculations were limited to electron energies of less than 10 keV, but here suprathermal electron energies of several tens of keV are to be studied. Furthermore, in order to avoid any influence of the high-energy border of the computational domain on the simulation results, the simulation box should cover energies of the order of 100 keV. Such energies require a relativistic treatment of the electrons.

The kinetic model is based on the solution of the Boltzmann-Vlasov equation

$$\frac{\partial f}{\partial t} + (\boldsymbol{v}\cdot\nabla)f + [m_\mathrm{e}\gamma\boldsymbol{g} - e(\boldsymbol{E} + \boldsymbol{v}\times\boldsymbol{B}]\cdot\frac{\partial f}{\partial \boldsymbol{p}} = \left(\frac{\delta f}{\delta t}\right)_\mathrm{Coul} + \left(\frac{\delta f}{\delta t}\right)_\mathrm{wh} \quad (1)$$

where $\boldsymbol{g}$ and $\boldsymbol{E}$ represent the gravitational and charge separation electric field, respectively; $\boldsymbol{B}$ is the background magnetic field, m_e is the electron rest mass, $\gamma = \sqrt{1 + p^2/(m_\mathrm{e}c)^2}$ is the Lorentz factor, and the terms on the right-hand side are diffusion terms due to Coulomb collisions and the resonant interaction of the electrons with whistler waves. The Coulomb collisions of the electrons with both electrons and protons are calculated by a Fokker-Planck equation based on the Landau collision integral (Ljepojevic & Burgess 1990). A detailed description of the whistler-electron interaction is presented below.

The Boltzmann-Vlasov Eq. (1) depends on three spatial and on three momentum coordinates. These are too many dimensions for a numerical solution, since the computational effort would be far too high. But the electron gyroperiod in a typical coronal magnetic field is much smaller than any other characteristic time scale, so the electron VDF can be assumed to be gyrotropic. This assumption not only eliminates one of the momentum coordinates, namely the phase angle of the gyromotion, but also reduces the spatial coordinates to a single coordinate, s, along the background magnetic field, $\boldsymbol{B}$.

The remaining momentum coordinates can be described as $(p_\parallel, p_\perp)$, the components parallel and perpendicular to $\boldsymbol{B}$, respectively. Such a coordinate system has been used for the velocity coordinates in Vocks et al. (2005). But such a coordinate system becomes problematic for higher electron energies and momenta, p. This is because the wave-electron interaction and the mirror force in a diverging magnetic field geometry both change the pitch-angles of electrons. If the simulation box is a rectangle in $(p_\parallel, p_\perp)$ space, then lines of constant p cross both the high-$p_\parallel$ and high-$p_\perp$ boundaries of the box at some high p. As a consequence, this section of the simulation box is strongly influenced by these boundaries, and the boundary conditions applied there. This can cause numerical instabilities and renders the simulation results useless. The use of p and the pitch-angle, θ, as momentum-space coordinates overcomes this issue.

The Coulomb collisions and the whistler wave phase speeds depend on plasma background parameters like densities, drift velocities, and temperatures of both ions and electrons. These parameters, as well as the magnetic field geometry, have to be provided by a background model. In this paper, the background is provided by a loop model as presented below.

The background model does not change during a simulation run, so the electrons that are described by the Boltzmann-Vlasov Eq. (1) can be regarded as test particles. The solution of Eq. (1) requires the definition of an initial condition for the electron VDF. Since it is the aim of this paper to demonstrate that the quiet solar corona is capable of producing a suprathermal electron population, a Maxwellian VDF with the same density, drift velocity, and temperature as in the background model is a good choice for the initial electron VDF. But a Maxwellian VDF rapidly approaches zero for electron energies of a few tens of keV, and shows strong gradients on a logarithmic scale that cause numerical problems. To overcome this difficulty, a kappa distribution

$$f_\kappa(p) = N_\mathrm{e}\frac{\Gamma(\kappa+1)}{\pi^{3/2}(2\kappa-3)^{3/2}p_\mathrm{th}^3\Gamma(\kappa-1/2)}\left(1 + \frac{p^2}{(2\kappa-3)p_\mathrm{th}^2}\right)^{-(\kappa+1)} \quad (2)$$

with electron density, N_e, and a "thermal momentum", $p_\mathrm{th} = \sqrt{m_\mathrm{e}k_\mathrm{B}T}$, is used instead, with a very high $\kappa = 80$. Note that a kappa distribution approaches a Maxwellian in the limit $\kappa \to \infty$.

After the initial condition has been defined, the temporal evolution of the numerical system is calculated by means of the Boltzmann-Vlasov Eq. (1), until a final steady state is reached.

2.1. Kinetic treatment of the resonant interaction between electrons and whistler waves

The resonant interaction between electrons and whistler waves is described within the framework of quasilinear theory (Kennel & Engelmann 1966). Only waves propagating parallel to the background magnetic field, i.e. along the coronal loop, are considered here. Then the quasilinear diffusion equation can be written in the form given by Marsch (1998). In a relativistic form, and using the coordinates (p, θ), it reads:

$$\left(\frac{\delta f}{\delta t}\right)_{\rm wh} = \frac{1}{p^2 \sin\theta}\left[\frac{\partial}{\partial p}\left(\alpha_{pp}\frac{\partial f}{\partial p} + \alpha_{p\theta}\frac{\partial f}{\partial \theta}\right) + \frac{\partial}{\partial \theta}\left(\alpha_{\theta p}\frac{\partial f}{\partial p} + \alpha_{\theta\theta}\frac{\partial f}{\partial \theta}\right)\right] \quad (3)$$

with the parameters

$$\begin{aligned} \alpha_{pp} &= \tfrac{1}{\tau} p^2 \sin^3\theta\, v_{\rm ph}^2 \\ \alpha_{p\theta} = \alpha_{\theta p} &= \tfrac{1}{\tau} p \sin^2\theta\, v_{\rm ph}\,(v_{\rm ph}\cos\theta - v) \\ \alpha_{\theta\theta} &= \tfrac{1}{\tau}\sin\theta\,(v_{\rm ph}\cos\theta - v)^2, \end{aligned} \quad (4)$$

the whistler wave phase speed, $v_{\rm ph}$, the electron speed, $v = p/(m_{\rm e}\gamma)$, and the "collision frequency" associated with the whistler-electron interaction:

$$\frac{1}{\tau} = \frac{\pi}{4}\Omega_{\rm e}^2 \left|\frac{v_{\rm ph} - v\cos\theta}{v_{\rm ph}}\right| \hat{\mathcal{B}}_\omega. \quad (5)$$

$\hat{\mathcal{B}}_\omega$ is the wave spectral energy density at the frequency ω, normalized to the magnetic field energy density, $B^2/(2\mu_0)$, and $\Omega_{\rm e}$ is the electron cyclotron frequency, $\Omega_{\rm e} = eB/m_{\rm e}$.

The electron momentum (p, θ) and the whistler wave frequency are connected through the resonance condition

$$\omega - k_\parallel p_\parallel/(m_{\rm e}\gamma) = \Omega_{\rm e}/\gamma. \quad (6)$$

$p_\parallel = p\cos\theta$ is the momentum component parallel to the background magnetic field, and $k_\parallel$ is the parallel wave vector component. The resonance condition states that the Doppler-shifted wave frequency in the reference frame of the electron equals the electron's gyrofrequency. The dispersion relation of whistler waves imposes an upper frequency limit, $\omega < \Omega_{\rm e}$. For the electron energies discussed in this paper, the Lorentz factor is small, $\gamma \approx 1$. Then the resonance condition has the consequence that $p_\parallel$ and $k_\parallel$ must have different signs. In principle, relativistic electrons can fulfil the resonance condition with equal signs of $p_\parallel$ and $k_\parallel$. But for typical coronal loop plasma conditions, even 100 keV electrons with $\gamma = 1.2$ can do so only for very small $p_\parallel \approx 10^{-3} m_{\rm e}\, c$ and wave frequencies close to the local electron cyclotron frequency, where the wave power already has been absorbed by the bulk of thermal electrons. So effectively, waves propagating in one direction only interact with electrons moving into the opposite direction.

The basic effect of the diffusion Eq. (3) on the electron VDF is pitch-angle diffusion in the reference frame of the waves. If the waves are sufficiently strong, the deformation of the VDF saturates in the formation of "kinetic shells" that are used by Isenberg et al. (2001) to model proton distributions in the solar corona and wind. As long as the wave phase-speed is small as compared to the electron thermal speed, $v_{\rm th}$, this interaction has the only consequence of forming an isotropic distribution. But if $v_{\rm ph}$ is much higher than $v_{\rm th}$, then electrons can be brought from small $p_\parallel$ to high $p_\perp$, leading to an increase of p. This is what the suprathermal electron production mechanism in Vocks & Mann (2003) is based on.

However, the region around $p_\parallel = 0$ is critical. For small γ, the resonance condition, Eq. (6), requires that the wave frequency, ω, approaches the electron gyrofrequency, $\Omega_{\rm e}$. Since whistler waves cannot propagate at this frequency, and most of the spectral wave power at frequencies $\omega \approx \Omega_{\rm e}$ has been absorbed by the electrons further down the loop, there is no wave power available, and the diffusion coefficient from Eq. (5) becomes very small, $1/\tau \approx 0$. So the model lacks an efficient diffusion mechanism across the line $p_\parallel = 0$. In the real corona, waves propagating obliquely to the background magnetic field can help to overcome this issue, but their consideration in the model would introduce a complicated integral over all wave vectors, $\boldsymbol{k}$ into the diffusion Eq. (3) (Marsch & Tu 2001). In order to alleviate this problem, the same diffusion as in Vocks et al. (2005) of $1/\tau$ across neighboring grid points along the pitch-angle coordinate is introduced for pitch-angles close to $\pi/2$.

2.2. Coronal loop background model

It has been pointed out above that the kinetic model for electrons needs a background model that provides densities, drift velocities, and temperatures of both protons and electrons. These data are necessary for calculating the Coulomb collisions, the whistler wave propagation inside the simulation box, and the charge-separation electric field. In this paper, the geometry of a coronal loop is used.

The loop geometry, i.e. the magnetic field, $B(s)$, and the angle $\psi(s)$ between $\boldsymbol{B}$ and the direction normal to the solar surface, is calculated from photospheric potential magnetic field extrapolation (e.g. Seehafer 1978; Sakurai 1982). The same algorithm is used as in Aurass et al. (2005). A photospheric dataset from the 28 Oct. 2003 has been used to reconstruct the loop, but for a region that is separated from the active region that produced the strong flare events of that day.

The "upper" and "lower" boundaries of the simulation box, with respect to the spatial coordinate along the loop, s, are located in the transition region. The temperature inside the loop is set to 1.4 MK for both electrons and protons, and the particle number densities at the coronal base is $N_{\rm e} = N_{\rm p} = 2 \times 10^{15}$ m^{-3}. Inside the loop, the pressure is hydrostatic, and there is no plasma flow along the loop.

Figure 1 shows the loop height, magnetic field, particle number densities, and temperatures for both electrons and protons as functions of s. The total length of the loop is 210 Mm, its maximum height is $z_{\rm max} = 63.5$ Mm at $s = 115$ Mm. The strong temperature and density gradients of the transition region are barely visible at the $s = 0$ Mm and $s = 210$ Mm edges of this plot. The borders of the simulation box are located at a temperature of 4×10^5 K. It clearly can be seen that the loop is not symmetric. The magnetic field at the loop footpoints is $B(s = 0\,\text{Mm}) = 137$ G and $B(s = 210\,\text{Mm}) = 92$ G, and the minimum value of B is not reached at the loop top, but at $s = 162$ Mm with $B_{\rm min} = 2.3$ G.

The whistler waves enter the coronal loop at both footpoints. The waves are assumed to be a high-frequency tail of the same wave spectrum that is discussed for coronal heating (e.g. Cranmer et al. 1999; Vocks & Marsch 2002). The ion cyclotron waves discussed in these papers are left-hand polarized, but it is reasonable to assume that not only left-hand, but also right-hand polarized waves, i.e. whistler waves, are present. The whistler wave spectrum is set up as a power law, $\mathcal{B}_\omega \propto \omega^{-\alpha}$, and the index α is set to 1.3. The total wave power is chosen in such a way that the total energy content of the full spectrum, from the 5-min oscillations up to the electron cyclotron frequency,

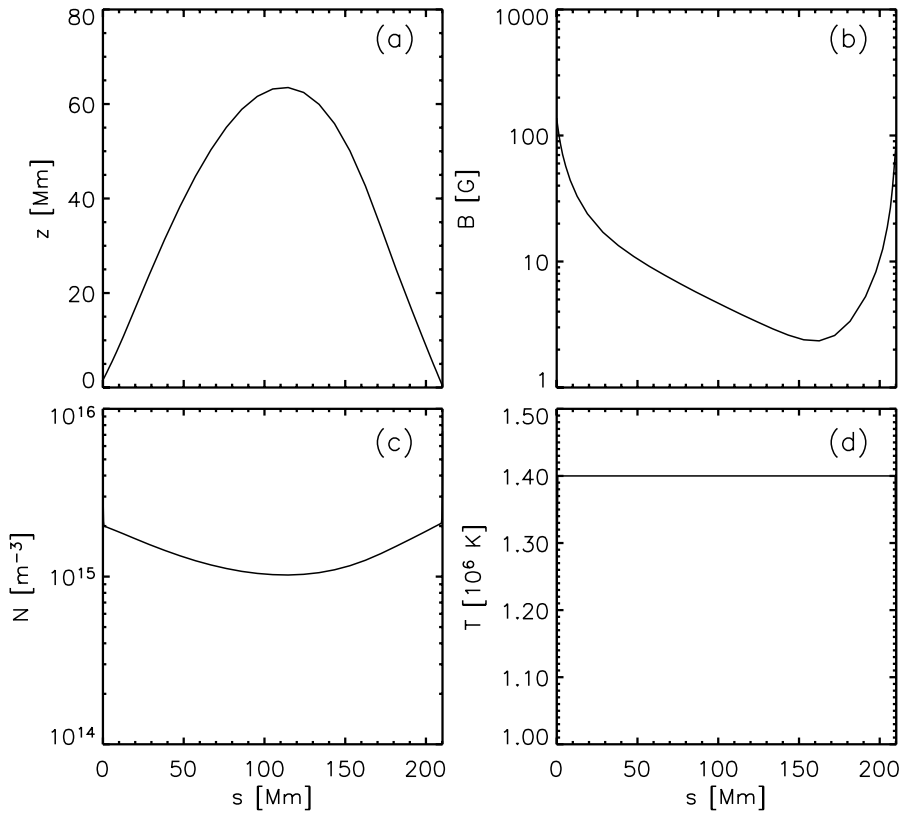

Fig. 1. The coronal loop background model. Shown are loop height, z, the magnetic field, B, and the particle number densities, N, and temperatures, T, as functions of the spatial coordinate, s, along the loop. Electrons and protons have the same densities, $N = N_e = N_p$, and temperatures, $T = T_e = T_p$.

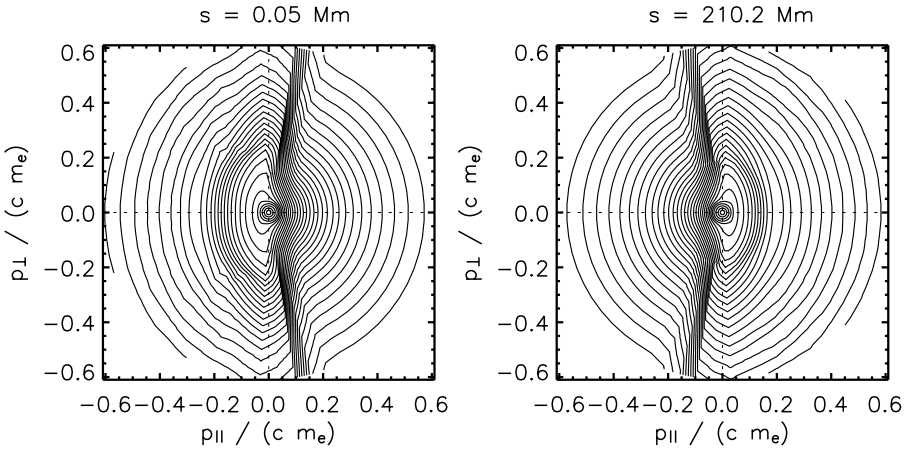

Fig. 2. Isoline plots of the electron VDFs close to the loop footpoints at $s = 0$ Mm (*left*) and $s = 210$ Mm (*right*). The spacing of the isolines has been chosen in such a way that they form equidistant circles for a Maxwellian VDF. The region with high isoline density marks the boundary between electrons that have entered the loop at the footpoints and electrons that have been mirrored inside the loop, as described in the text.

corresponds to a wave energy flux density of 275 Wm^{-2} (Hollweg 2006). The waves propagate into the loop, and the evolution of the wave spectrum due to the spatial variation of the phase speed and the absorption by electrons are considered in the model.

3. Results

The numerical solution of the Boltzmann-Vlasov Eq. (1) is performed for the coronal loop presented in the previous section, Fig. 1. The electron momentum range covers values up to $p_{max} = 0.6\, m_e\, c$, that corresponds to energies of up to 100 keV. The total simulation time is 80 s. This allows electrons with thermal speed to travel from one footpoint to the other one, and back. So the time is long enough to let the numerical system "forget" its initial condition, and indeed it has reached a final steady state.

The results presented in this paper have been obtained with a grid spacing of the momentum coordinate of $\Delta p = 2000\,\mathrm{km\,s^{-1}}\, m_e$. This is less than half of the thermal speed inside the loop, and fine enough to study the formation of suprathermal VDF tails. In order to ensure that the results shown here are indeed based on whistler-electron interaction, and are not an artifact due to numerical diffusion in momentum space, the calculation has been re-run with a finer $\Delta p = 1500\,\mathrm{km\,s^{-1}}\, m_e$, since numerical diffusion strongly depends on Δp. The results do not differ significantly.

Figure 2 shows the resulting electron VDFs at both loop footpoints, $s = 0$ Mm and $s = 210$ Mm. The VDFs clearly demonstrate the effect of the resonant interaction with whistler waves. At $s = 0$ Mm, the waves enter the loop with wavenumbers $k_\parallel > 0$, and from the resonance condition, Eq. (6), it follows that only electrons with $p_\parallel < 0$ can interact with these waves.

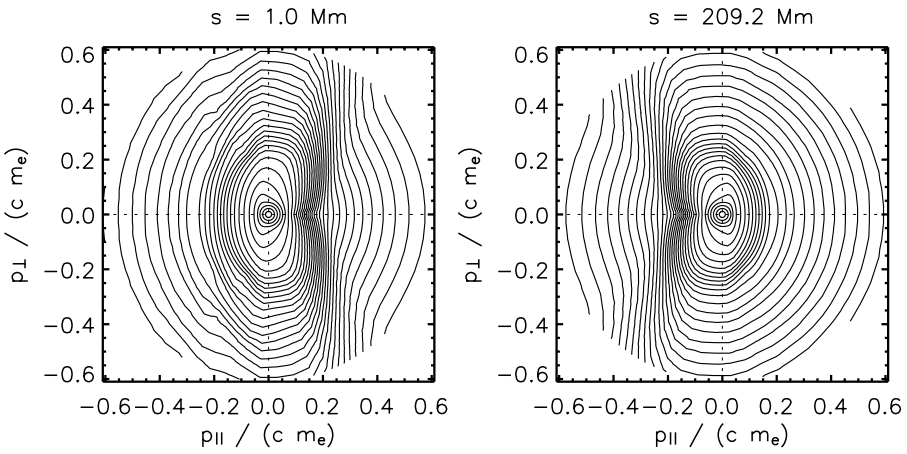

Fig. 3. Isoline plots of the electron VDFs at heights of 1 Mm above the loop footpoints. The spacing of the isolines is the same is in Fig. 2, and the high isoline density between electrons trapped inside the loop and having entered it through the footpoints is still visible.

The deformation of the VDF towards "kinetic shells" in this momentum range can clearly be seen in the left part of the figure. At the $s = 210$ Mm footpoint, the whistler waves entering the loop propagate towards smaller s. Thus, $k_\parallel < 0$, and the resonance condition requires $p_\parallel > 0$. The corresponding "kinetic shells" can be seen in the right part of Fig. 2. These deformations of initially isotropic VDFs demonstrate that electron acceleration is happening. As an example, it can be seen that electrons are diffused from $(p_\parallel = -0.15\, m_e\, c, p_\perp = 0)$ to $(p_\parallel = 0, p_\perp = 0.3\, m_e\, c)$, which corresponds to a 4-fold increase of energy.

The sections of electron momentum space that are not affected by the whistler-electron interaction, i.e. $p_\parallel > 0$ at $s = 0$ Mm and $p_\parallel < 0$ at $s = 210$ Mm, respectively, are populated by electrons that just have entered the loop through the footpoint boundaries. Their VDFs are close to the kappa distributions, with $\kappa = 80$ and transition region densities and temperatures, that are used as spatial boundary conditions of the simulation box, and do not show pronounced suprathermal tails. As a consequence, a strong phase-space density gradient develops at the boundary between these two electron populations, that can be seen as a region with high isoline density in the figure.

Inside the coronal loop, the VDFs evolve further. Figure 3 shows that with increasing height above the transition region, the mirror force in the widening loop (cf. Fig. 1b) pushes the electrons towards positive $p_\parallel$ ($s = 1$ Mm) and negative $p_\parallel$ ($s = 209$ Mm), respectively. These suprathermal electrons then propagate towards the loop top region. Due to this process, some loss-cone structures form that potentially could lead to whistler-wave excitation (Scharer & Trivelpiece 1967; Mann et al. 1989). But considering such plasma instabilities is beyond the scope of the model calculations presented here. The phase-space densities of the loss-cone regions are also relatively low, so that the wave growth would be quite weak.

At the loop top, the electron VDF is more isotropic, as shown in Fig. 4. This is expected, since the suprathermal electrons from both footpoints reach this region. The whistler-electron interaction weakens here, since the magnetic field and thus the electron gyrofrequency barely changes with s, and most of the spectral wave power has been absorbed further down, closer to the footpoints. The VDF is not perfectly symmetric, since the loop itself is asymmetric, see Fig. 1.

Two components of the electron VDF can be distinguished, a thermal core and an extended halo. The thermal core forms due to the strong Coulomb collisions in the dense coronal loop, along with the weak local wave-electron interaction. The temperature of the core equals that of the background model, $T = 1.4$ MK. So

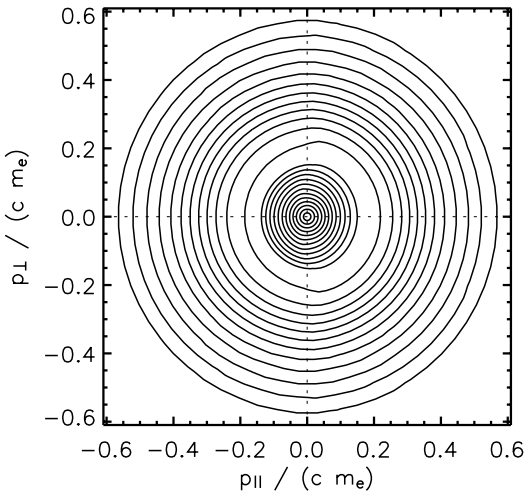

Fig. 4. Isoline plots of the electron VDFs at the loop top, $s = 115$ Mm. The spacing of the isolines is the same is in Fig. 2.

it is apparent that a halo of suprathermal electrons has formed, in excess of the thermal population.

For a further study of this suprathermal tail, Fig. 5 shows a plot of the pitch-angle average electron VDF at the loop top, $s = 115$ Mm. The thermal core and the deviation of the halo distribution from a Maxwellian VDF are clearly visible. The thermal core extends up to an electron momentum of about $p = 0.125\, m_e\, c$, that corresponds to an energy of 4 keV. This is a consequence of the high density in the coronal loop. Above this energy, the halo distribution becomes visible. It can roughly be approximated by a double power-law. At low energies, up to about $p = 0.2\, m_e\, c$ (10 keV), it is relatively flat, but at higher energies up to the full 100 keV, it becomes steeper.

The energy range below 10 keV is of special interest, since it allows for a direct comparison of the simulation results with the solar wind measurements of Maksimovic et al. (1997b). Figure 6 shows the pitch-angle average VDF at lower energies, together with a power-law fit, $p^{-\alpha}$, with index $\alpha = 10$. According to the definition of the kappa function, Eq. (2), this corresponds to a $\kappa = 4$ for suprathermal energies. The fit of the electron VDF by the power law is very good in the momentum range $p = 0.15$–$0.2\, m_e\, c$, that just corresponds to energies of

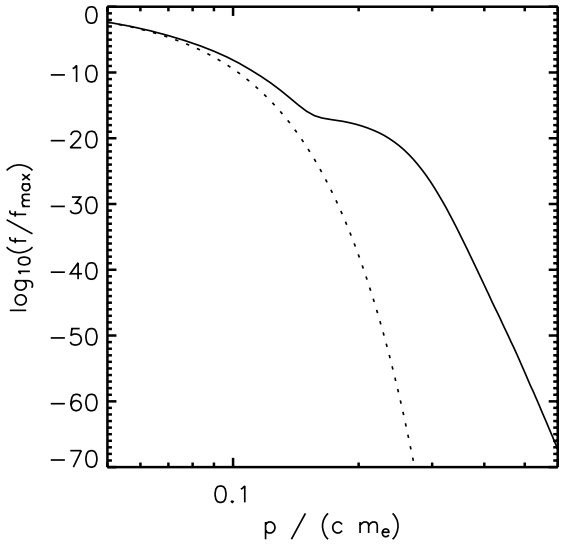

Fig. 5. Pitch-angle average electron VDF at the loop top, $s = 115$ Mm. The dotted line is a Maxwellian VDF with the same density and temperature.

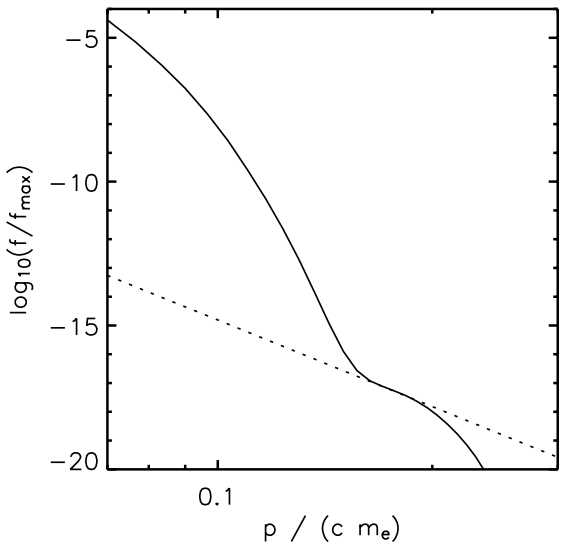

Fig. 6. Pitch-angle average electron VDF at the loop top, $s = 115$ Mm, for low energies. The dotted line is a power-law, $p^{-\alpha}$, with $\alpha = 10$.

6–10 keV, which are relevant for the comparison with solar wind measurements.

3.1. The influence of the high-p boundary condition

For low energies of less than 10 keV, the suprathermal electron halo distribution starts with a relatively small power-law index. But for higher energies above 10 keV, the slope of the VDF becomes steeper, as shown in Figs. 5 and 6. This raises the question of why the suprathermal electron production becomes less efficient at higher energies.

There are several potential reasons for the relatively low number of electrons at higher energies. One is the acceleration mechanism through diffusion along "kinetic shells" itself. The energy gain connected with the electron transport from low $p_\parallel$ to high $p_\perp$ depends on the ratio between the wave phase speed, $v_{\rm ph}$,

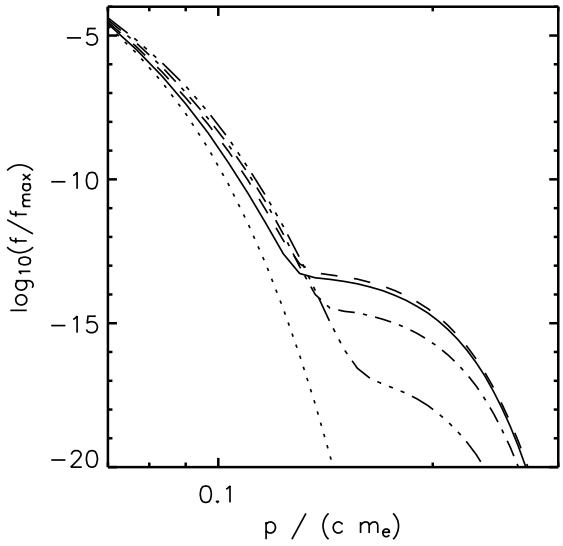

Fig. 7. Pitch-angle average electron VDF at the loop top, $s = 115$ Mm, for low energies. Shown are the results of simulation runs with $p_{\rm max}/(m_{\rm e}c) = 0.6$ (dash-dot-dot-dotted line), 0.8 (dash-dotted line), 1.0 (dashed line), and 1.2 (solid line), as well as a Maxwellian VDF (dotted line).

and electron speed, v. A high $v_{\rm ph}/v$ leads to a strong energy gain, but with increasing electron energy, v also increases, and the electron energy gain decreases. On the other hand, electrons in the coronal loop are reflected by the mirror force in the converging magnetic field geometry at the footpoints. The faster they are, the more acceleration cycles they can undergo in a given time interval. But electrons with sufficiently small pitch-angles are not mirrored, and escape from the loop into the transition region and chromosphere. So faster electrons can have a higher escape rate.

But not only the footpoints, i.e. the spatial boundaries of the simulation box, can influence the results. At a first glance, an electron energy range of 100 keV in the simulation seems to be enough for a discussion of the electron VDF at 10 keV. But from the "kinetic shells" in Figs. 2 and 3 it can be seen that the high-p boundary of the simulation box does influence the deep interior of the box. The pitch-angle diffusion in the wave reference frame transports electrons from relatively low $p_\parallel = 0.2\, m_{\rm e}\, c$ towards the high-p boundary at a pitch-angle close to $\pi/2$. So the boundary condition, which is an extrapolation based on the $\kappa = 80$ distribution used as the initial condition, is directly connected to the results for 10 keV electrons. So it is necessary to extend the range of p to avoid the boundary influence.

Figure 7 shows the resulting pitch-angle average electron VDFs at the loop top for multiple simulation runs with subsequently increased momentum ranges, $p_{\rm max}/(m_{\rm e}c)$. For the lowest value of 0.6, the plot is identical to Fig. 6. An increase to $p_{\rm max}/(m_{\rm e}c) = 0.8$ leads to a strong increase of the VDF in the range $p/(m_{\rm e}c) = 0.15$–0.25. This is in agreement with the finding that the "kinetic shells" at the loop footpoints connect $p = 0.2\, m_{\rm e}\, c$ with the high-p boundary for $p_{\rm max}/(m_{\rm e}c) = 0.6$. The extension of the momentum range alleviates the influence of the boundary condition considerably. A further extension to $p_{\rm max}/(m_{\rm e}c) = 1.0$ leads to an additional increase of the electron VDF around $p = 0.2\, m_{\rm e}\, c$, but then it saturates. Increasing $p_{\rm max}$ further to $1.2\, m_{\rm e}\, c$ does not influence the result. So it can be concluded that the simulation results for suprathermal electrons are

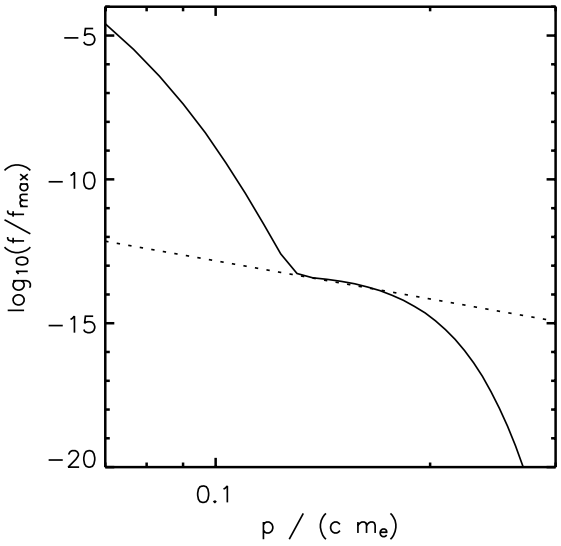

Fig. 8. Pitch-angle average electron VDF at the loop top, $s = 115$ Mm, for low energies. The dotted line is a power-law, $p^{-\alpha}$ with $\alpha = 4.4$.

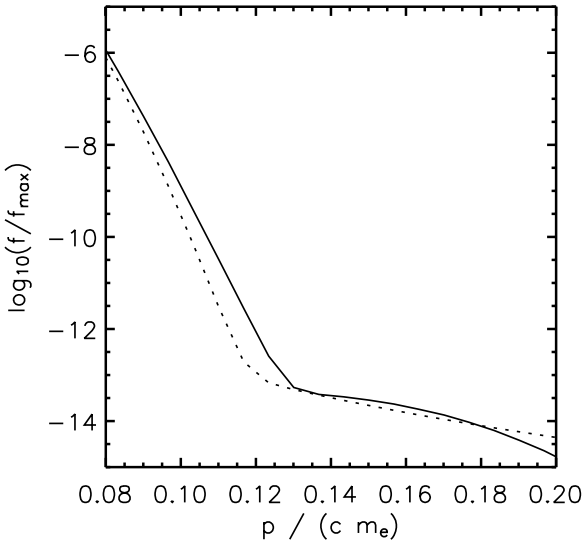

Fig. 9. Pitch-angle average electron VDF at the loop top, $s = 115$ Mm, for low energies. The dotted line is a Maxwellian + kappa distribution with $\kappa = 1.8$ and density $N_\kappa = 3 \times 10^{-9}\, N_e$.

not affected any longer for this high momentum range that corresponds to a maximum energy of 287 keV in the model.

A comparison of the model results for $p_{max}/(m_e c) = 0.6$ and $p_{max}/(m_e c) = 1.2$ in Fig. 7 shows that the former strongly underestimates the production of suprathermal electrons in the loop. So the analysis of the suprathermal population from the previous sub-section should be repeated for the $p_{max}/(m_e c) = 1.2$ result.

Figure 8 shows this electron VDF in the same style as in Fig. 6, together with a power-law fit, $p^{-\alpha}$. But here the index can be set as low as $\alpha = 4.4$. This is so low that it is not possible to calculate a corresponding κ. The term $(2\kappa - 3)$ in the definition of the kappa distribution, Eq. (2), requires that $\kappa > 1.5$. For high p, the kappa distribution turns into a power-law $p^{-2(\kappa+1)}$, so that a minimum $\alpha = 5$ is required for the definition of a corresponding κ. So this calculation demonstrates that the electron VDF can develop suprathermal tails which are stronger than can be described by a κ distribution.

The suprathermal electron population is now much stronger as compared to Fig. 6, with higher phase-space densities, and it separates from the thermal core at a lower momentum $p = 0.13\, m_e\, c$, which corresponds to an electron energy of about 4 keV. So the power-law fit is now valid for the energy range of 4–10 keV, as compared to 6–10 keV in Fig. 6. So the previous calculation did indeed underestimate the suprathermal electron production.

Figure 9 shows the same electron VDF as in Fig. 8, together with a fit by a combined Maxwellian and kappa distribution. The Maxwellian VDF corresponds to the background plasma in the loop. The kappa distribution has a $\kappa = 1.8$ and a density of 3×10^{-9} times the background electron density, N_e. This is $N_\kappa = 3 \times 10^6\ \mathrm{m}^{-3}$ in absolute units. The thermal momentum, p_{th}, of the kappa component corresponds to the background temperature, $T = 1.4$ MK, but the fit is very insensitive to this parameter.

This fit of the VDF with a combined core and kappa distribution resembles the solar wind analysis of Maksimovic et al. (1997b). The low kappa value is in good agreement with their results. But the electron energies where the kappa component becomes apparent are much higher here. This is due the strong Coulomb collisions in the dense coronal loop. Electrons with energies below 4 keV are quickly thermalized. The kink of the VDF at $p = 0.13\, m_e\, c$ clearly shows that the slower electrons are collision dominated. The diffusion of electrons in momentum space due to the Coulomb collisions can also be responsible for the deviation between the electron VDF and the combined core + kappa distribution around $p = 0.12\, m_e\, c$.

3.2. Results with coronal funnels

The electrons in the model calculations presented here are confined to a coronal loop. If they approach a loop footpoint, they experience a mirror force in the converging magnetic field towards the footpoint. The force arises from the conservation of magnetic momentum. If the initial pitch-angle is sufficiently large, the electrons are reflected back into the loop. But electrons with small enough pitch-angles can escape from the loop towards the transition region and chromosphere.

So the quality of the magnetic confinement determines what fraction of the electrons can escape the loop at each footpoint. The pitch-angle diffusion of the electrons due to resonant interaction with whistler waves complicates the picture, since it modifies the magnetic momentum, but generally the electrons are better confined if the magnetic field converges more strongly at the footpoints.

The electron pitch-angle diffusion in the wave reference frame, and the associated electron acceleration, can be seen in Fig. 2. Electrons with sufficiently large pitch-angles are mirrored back into the loop, as it is evident from Fig. 3, that shows the electron VDFs at a slightly larger height in the loop. These electrons move through the interior of the loop, and eventually approach the other footpoint. There they interact with the whistler waves entering at this footpoint. The diffusion and the mirror force in the given magnetic field geometry again determine what fraction of them is reflected back into the loop, and what fraction leaves the loop. Those electrons that are reflected move back towards the first footpoint, where they are again mirrored and diffused, and so on. So electrons can undergo multiple such cycles, and be accelerated at each footpoint passage. This leads to an enhancement of the suprathermal tails, but eventually an

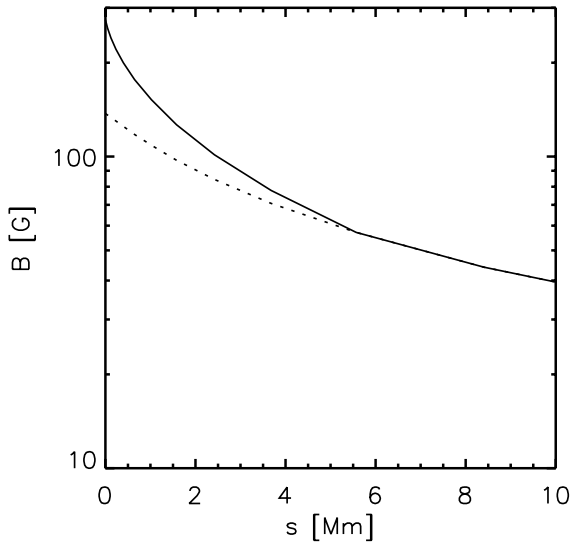

Fig. 10. Modified loop geometry as a function of the spatial coordinate, s, along the loop. Shown are the new, stronger magnetic field, B (solid line), and the previously used model (dotted line). The same increase of the magnetic field is applied to the $s = 210$ Mm footpoint.

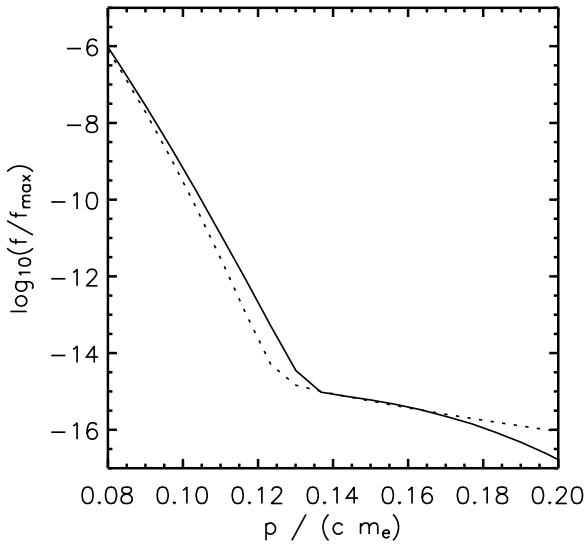

Fig. 12. Pitch-angle average electron VDF at the loop top, $s = 115$ Mm, for low energies. The dotted line is a Maxwellian + kappa distribution with $\kappa = 2.2$ and density $N_\kappa = 1 \times 10^{-10}\, N_e$.

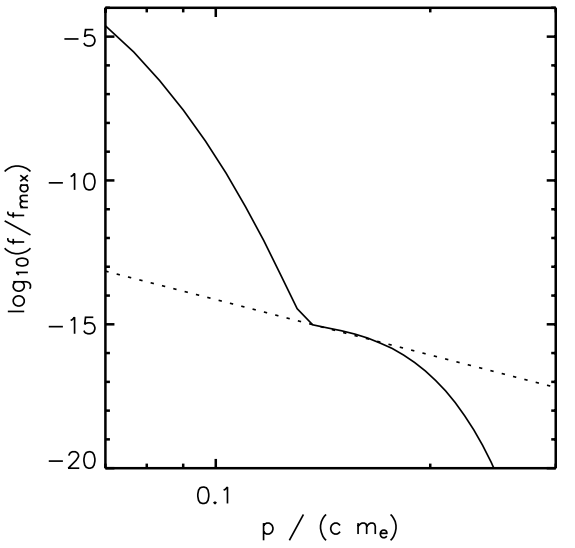

Fig. 11. Pitch-angle average electron VDF at the loop top, $s = 115$ Mm, for low energies. The dotted line is a power-law, $p^{-\alpha}$ with $\alpha = 6.4$.

equilibrium with the losses due to imperfect magnetic confinement is reached.

This raises the question of what influence the quality of the confinement, i.e. the increase of the magnetic field toward the loop footpoints, has on the simulation results. To investigate this, the simulation is run again for a loop where the magnetic field increases within 4 Mm of the footpoints to the two-fold value as compared with the previously used loop geometry.

Figure 10 shows the new magnetic field as a function of the loop length, s. For the $s = 210$ Mm footpoint, a similar increase of B is applied. Such a rapid increase of the magnetic field towards the transition region resembles a coronal funnel.

Figure 11 displays the simulation result for the new magnetic field geometry in the same style as in Fig. 8, together with a power-law fit, $p^{-\alpha}$. The better magnetic confinement in this simulation run might lead to the assumption that the suprathermal tails of the electron VDFs are stronger here. But the somewhat surprising result is that they are actually weaker. The power-law index has increased to a steeper $\alpha = 6.4$, and the overall phase space density is lower.

A fit of the new electron VDF to a combined Maxwellian and kappa distribution confirms this finding. The value $\kappa = 2.2$ is in agreement with the power-law index $\alpha = 6.4$ from above, since $\alpha = 2(\kappa+1)$ according to the definition of the kappa distribution, Eq. (2). The density of the kappa population is only 10^{-10} of the total electron density, N_e. This is much less than the $3 \times 10^{-9}\, N_e$ in the previous simulation run.

So it has to be concluded that the the electron acceleration is now much less efficient despite the better confinement of the electrons in the loop. The reason for this is the higher magnetic field, B, close to the loop footpoints. A higher B leads to a higher electron cyclotron frequency, $\Omega_e = eB/m_e$, and thus the resonance frequencies of the electrons are also higher. Since the whistler waves enter the simulation box with a power-law spectrum $\propto\omega^{-1.3}$, there is less wave power available for electron acceleration close to the loop footpoints. But the region close to the footpoints is where the wave phase speeds are highest, and high phase speeds are necessary for an efficient electron acceleration from low $p_\perp$ to high $p_\parallel$, cf. Fig. 2. The minimum value of B in the simulation box has not been changed, so in total there is not less wave energy available for absorption by the electrons in this simulation run than before, but most of it is shifted now further away from the footpoints, where the acceleration is less effective.

So the weaker electron acceleration cancels the effect of the better magnetic confinement of the suprathermal electrons inside the loop. The reason for the weak acceleration is the strong magnetic field at the footpoints, that leads to low wave power at electron resonance frequencies. To overcome this issue, another simulation run has been performed, with B reduced by half. So

now the magnetic field at the footpoints is the same as in the first simulations, Fig. 1a, and it is reduced to half of its original value inside the loop. But this simulation also resulted in a lower number of suprathermal electrons as compared to Figs. 8 and 9. This is due to the reduced wave phase speeds, that decrease rapidly close to the footpoints as B is reduced. Lower wave speeds mean less efficient electron acceleration, and even at low heights in the loop the electrons are pitch-angle scattered, but hardly accelerated.

These studies show that the suprathermal electron population inside the loop does depend on the loop geometry. But there is no simple recipe for strong suprathermal tails. Their formation is a compromise between efficient acceleration, that requires a strong magnetic field for high whistler-wave phase-speeds, and available wave power, that requires a not too strong B due the power-law nature of the wave spectrum, which provides less wave energy for higher frequencies.

4. Conclusions and summary

The simulation results presented in this paper show that the quiet solar corona is capable of producing pronounced suprathermal tails of electron VDFs. The suprathermal tails can be fitted by a power-law, $\propto p^{-\alpha}$, and the index can be as small as $\alpha < 3$. For energies up to 10 keV, the coronal electron VDF can also be fitted with a combined Maxwellian + kappa distribution, with κ as small as $\kappa = 1.8$.

The acceleration mechanism is based on pitch-angle diffusion of the electrons in the reference frame of coronal whistler waves, i.e. diffusion along "kinetic shells". This mechanism has the consequence that the high-p boundaries of the simulation box can influence the results inside the box even at relatively low energies. So care must be taken here. It has been shown that it is necessary to extend the simulation to higher energies than anticipated.

The magnetic field geometry also influences the efficiency of suprathermal electron production. Since the whistler waves are assumed to have a power-law spectrum with less energy at higher frequencies, the wave power depends on the electron resonance frequencies, that are close to the gyrofrequency. So a stronger magnetic field leads to less efficient electron acceleration. Furthermore, the variation of the magnetic field inside the simulation box determines the range of the whistler wave spectrum that can provide energy for electron acceleration, and a stronger variation leads to better confinement of the suprathermal electrons in the coronal loop. So a strong variation should lead to more suprathermal electrons. But it has been found that this is not necessarily the case. Either a strong magnetic field at the footpoints leads to less efficient acceleration there, or a low field inside the loop turns the "kinetic shell" formation into mere pitch-angle scattering without much electron acceleration. So a modification of the loop geometry simultaneously has opposite effects on the electron acceleration.

This paper focuses on the acceleration process of suprathermal electrons, starting from a nearly Maxwellian VDF. Thus, a closed volume of coronal plasma is studied. But what are the consequences of these results for solar wind electron VDFs?

Electrons in the fast solar wind originate from open magnetic field geometries that are not considered here, but magnetically closed regions in the corona are the sources of the slow solar wind. Maksimovic et al. (1997a) have found pronounced kappa tails not only in fast, but also in slow solar wind electron VDFs. So the simulation results are in agreement with observations so far, although the model does not include any mechanism for releasing suprathermal electrons from the loop into interplanetary space. But no magnetic confinement is perfect, although the details of the escape mechanism can influence the relation between the electron VDFs in a closed loop and in the slow solar wind. As a rough comparison between model calculations and observations, take the density of suprathermal electrons in the model loop, which has been found to be $N_\kappa = 3 \times 10^6\,\mathrm{m}^{-3}$. If this population could propagate freely into the solar wind, and if the electron flux is conserved along a magnetic field line, then the electron density would be reduced by the expansion factor of the magnetic field from the corona into the solar wind. The magnetic field in the model corona is 2.4 G, and a typical solar wind magnetic field is 5×10^{-5} G. Thus, the solar wind suprathermal electron density would be $60\,\mathrm{m}^{-3}$. This is much less than the $10^5\,\mathrm{m}^{-3}$ found by Maksimovic et al. (1997a), but in the dense model loop all electrons with energies below 4 keV are thermalized quickly by Coulomb collisions. This leads to a reduction of the suprathermal electron population in the dense loop studied here. For a study of magnetic field structures that are open towards interplanetary space, i.e. a coronal hole and fast solar wind, this effect should be much smaller. Such a coronal hole/solar wind model will be the subject of future work.

For electron energies above 10 keV, the electron VDF deviates from the power-law and falls off more rapidly, as can be seen in Figs. 8 and 11. So the superhalo component of solar wind electron VDFs, as observed by Lin (1998), is not produced here and must have a different origin. The reason for the low number of suprathermal electrons in the range of a few tens of keV lies in the velocity dependence of the acceleration mechanism. The efficiency of the acceleration by diffusion along "kinetic shells" depends on the ratio between the wave phase speed, v_{ph}, and electron speed, v. As v is increased, this ratio declines, and the diffusion process resembles more and more pure pitch-angle diffusion without much energy gain for the electrons. More wave power does not change the result very much either. As soon as the electron VDF has reached a kinetic shell form, see Fig. 2, the acceleration mechanism is saturated. The resulting electron energy spectrum is determined by the electron movement along the loop, together with the spatial variation of the wave phase speeds, and thus of the "kinetic shells". So the loop and magnetic field geometry does influence the details of the result, as shown in the last section, but the qualitative picture with less efficient acceleration at higher energies is quite robust.

It would be interesting to study observable consequences of coronal suprathermal electron populations as presented in this paper. Here, significant deviations between the model VDFs and a Maxwellian are found at energies above 5 keV up to 10 keV. So X-ray spectroscopy of the quiet solar corona should be capable of determining whether such suprathermal tails really do exist. RHESSI quiet sun observations by Hannah et al. (2007) recently have shown that the X-ray emission in the 3–6 keV energy range is in agreement with a coronal temperature of about 6 MK, which is much higher than the typical value of coronal electron temperatures of 1–2 MK. From the suprathermal tails that have been found in this study, an enhancement of the emission in the energy range above 5 keV would be expected. However, suprathermal tails of the electron VDF are not the only explanation for such an observation, e.g. a contribution from nanoflares would have the same effect. But spectroscopic studies of the quiet solar X-ray emission are an interesting topic for future research.

Acknowledgements. This work was supported by the German *Deutsche Forschungsgemeinschaft, DFG* project number MA 1376/17-1.

References

Aurass, H., Rausche, G., Mann, G., & Hofmann, A. 2005, A&A, 435, 1137
Axford, W. I., McKenzie, J. F., Sukhorukova, G. V., et al. 1999, Space Sci. Rev., 87, 25
Cranmer, S. R., Field, G. B., & Kohl, J. L. 1999, ApJ, 518, 937
Dorelli, J. C., & Scudder, J. D. 2003, J. Geophys. Res., 108, doi:10.1029/2002JA009484
Hannah, I. G., Hurford, G. J., Hudson, H. S., Lin, R. P., & van Bibber, K. 2007, ApJ, 659, L77
Hollweg, J. V. 2006, J. Geophys. Res., 111, doi:10.1029/2006JA011917
Isenberg, P. A., Lee, M. A., & Hollweg, J. V. 2001, J. Geophys. Res., 106, 5649
Kennel, C. F., & Engelmann, F. 1966, Phys. Fluids, 9, 2377
Leubner, M. P. 2004, ApJ, 604, 469
Lie-Svendsen, Ø., & Leer, E. 2000, J. Geophys. Res., 105, 35
Lie-Svendsen, Ø., Hansteen, H. V., & Leer, E. 1997, J. Geophys. Res., 102, 4701
Lin, R. P. 1980, Sol. Phys., 67, 393
Lin, R. P. 1998, Space Sci. Rev., 86, 61
Ljepojevic, N. N., & Burgess, A. 1990, Proc. R. Soc. Lond. A, 428, 71
Maksimovic, M., Pierrard, V., & Riley, P. 1997a, Geophys. Res. Lett., 24, 1151
Maksimovic, M., Pierrard, V., & Lemaire, J. F. 1997b, A&A, 324, 725
Mann, G., Baumgaertel, K., Chernov, G. P., & Karlický, M. 1989, Sol. Phys., 120, 383
Marsch, E. 1998, Nonlinear Proc. in Geophys., 5, 111
Marsch, E., & Tu, C.-Y. 2001, J. Geophys. Res., 106, 227
Pierrard, V., Maksimovic, M., & Lemaire, J. 1999, J. Geophys. Res., 104, 17021
Pilipp, W. G., Miggenrieder, H., Montgomery, M. D., et al. 1987, J. Geophys. Res., 92, 1075
Sakurai, T. 1982, Sol. Phys., 76, 301
Scharer, J. E., & Trivelpiece, A. W. 1967, Phys. Fluids, 10, 591
Scudder, J. D. 1992a, ApJ, 398, 299
Scudder, J. D. 1992b, ApJ, 398, 319
Seehafer, N. 1978, Sol. Phys., 58, 215
Vocks, C., & Marsch, E. 2002, ApJ, 568, 1030
Vocks, C., & Mann, G. 2003, ApJ, 593, 1134
Vocks, C., Salem, C., Lin, R. P., & Mann, G. 2005, ApJ, 627, 540,